

Supporting Information

Concomitant Polymorphs: An Alternative to Modulate Oxygen Evolution Reaction Performance of Mononuclear Nickel Complex

Chen Hu,¹ Qing-qing Huang,¹ Hai-Bing Xu,^{*1,2} Yuexing Zhang,¹ Xu Peng,¹ and
Ming-Hua Zeng^{*1,3}

1 Ministry-of-Education Key Laboratory for the Synthesis and Application of Organic Functional Molecules, Hubei Collaborative Innovation Center for Advanced Organic Chemical Materials, College of Chemistry and Chemical Engineering, Hubei University, Wuhan 430062, China. Corresponding Author.

2 State Key Laboratory of Structural Chemistry, Fujian Institute of Research on the Structure of Matter, Chinese Academy of Sciences, Fuzhou, Fujian 350002 (China).

3 Department of Chemistry and Pharmaceutical Sciences, Guangxi Normal University, Key laboratory for the Chemistry and Molecular Engineering of Medicinal Resources, Guilin, 541001, P.R. China.

E-mail: xhb@hubu.edu.cn; zmh@hubu.edu.cn

Contents

Table S1	Strategy of transition metal complexes as electrocatalysts for OER.
Table S2	DFT calculation on the coordinating OH ⁻ mode of NiL₂-R and NiL₂-G .
Table S3	Gibbs free energy of NiL₂-R and NiL₂-G on different steps of OER under U=0V and U=1.0 V.
Figure S1	Gibbs free energy level diagram of different steps of OER on NiL₂-R .
Figure S2	Gibbs free energy level diagram of different steps of OER on NiL₂-G .
Figure S3	Half CVs of (a) NiL₂-G and (b) NiL₂-R electrodes in aqueous solutions with different pH values (the scan rate is 10mV/s). And the dependent potentials of (c) NiL₂-G and (d) NiL₂-R on pH values.
Figure S4	DSC curves (Normalized) of NiL₂-R than that of NiL₂-G .
Figure S5	CVs for NiL₂-G and NiL₂-R treated at 140 °C for 2 hours.
Figure S6	CVs were measured in the non-faradaic region of 0.10–0.20 V vs. Ag/AgCl with different scan rates, varying from 20 mV s ⁻¹ to 120 mV s ⁻¹ .
Figure S7	85% IR-corrected polarization LSV curves in 1.0 M KOH at a scan rate of 10 mV/s for CB@NiL₂-G and CB@NiL₂-R .
Table S3	Comparison of the parameters in our work with other reported examples.
Figure S8	NiL₂-R soaked in KOH solution for 10 hours.
Figure S9	UV-vis absorption spectra along with the time for NiL₂ (1mg) dissolved in a mixture solvent of DMF (1mL) and KOH solution (9mL).
Figure S10	Stability check of NiL₂ by 500 cycles of CV scans in a 1 M KOH representing the (red) 2 nd and (black) 500 th cycles of the CV scan of NiL₂-G (a) and NiL₂-R (b). Inset: Enlarged region of the same voltammograms showing only a 50 μA difference for NiL₂-G and 70 μA difference for NiL₂-R in the catalytic current.
Figure S11	Chronopotentiometric measurements of NiL₂-G and NiL₂-R for 4000 seconds with a current density of 10mA/cm ² .
Figure S12	UV-vis absorption spectra of electrode materials dissolved in DMF before and after catalysis, show no obvious change in the curve.
Figure S13	UV-vis absorption spectra of (a) the electrolyte and (b) the centrifuged products of electrolytes dissolved in DMF after catalysis.
Figure S14	PXRD spectra for pure carbon paper, NiL₂-G before and after catalysis, NiL₂-R before and after catalysis.
Figure S15	Comparison of the Ni 2p high-resolution XPS survey spectrum of NiL₂-G (right) and NiL₂-R (left) before and after electrocatalysis; The satellite peaks are indicated by an asterisk (*).

Characterization

UV-vis absorption spectra were measured on an Agilent Cary6000i UV-VIS-NIR spectrophotometer.

Powder X-ray diffraction (PXRD) spectra were recorded on either a D8 Advance (Bruker) or a Rigaku D/max-III A diffractometer (Cu K α , $\lambda = 1.54056 \text{ \AA}$) at 293 K. Transmission electron microscopy (TEM) images of the samples were obtained using a FEI Talos F200X transmission electron microscope (200 kV).

X-ray photoelectron spectroscopy (XPS) were measured on a Thermo Escalab 250xi X-ray photoelectron spectrometer.

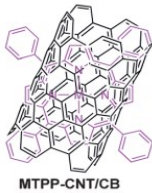
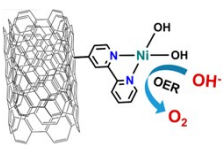
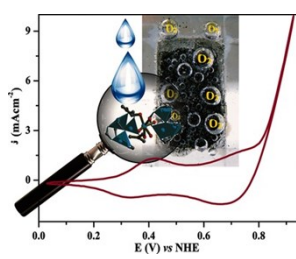
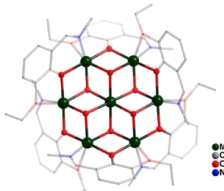
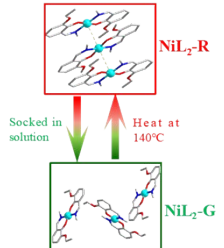
Density Functional Theory (DFT) calculation was carried out to study the mechanism of nickel-catalyzed oxygen evolution. All calculations were carried out with the gaussian16,^[1] B3LYP functional adding GD3BJ empirical dispersion, SDD ESP for Ni and 6-311G(d) basis set for other elements. The relationship between Boltzmann energy distribution and Gibbs free energy distribution: $G = -kT \ln q^N + NkTV(\partial \ln q / \partial V)_T$, N represents the number of particles in the system, K represents the Boltzmann constant, T represents the thermodynamic temperature, q represents Partition function of particles, V represents Molecular velocity vector.

Electrochemical tests:

The electrochemical and electrocatalytic properties of the materials toward OER were comprehensively evaluated with a traditional three-electrode configuration using an electrochemical station (CHI 760E) in 1 M KOH solutions at room temperature. In our case, carbon paper uniformly coated with the electrocatalysts was used as the working electrode, an Ag/AgCl (saturated KCl solution) electrode was used as reference electrode, while the counter electrode was a Pt electrode. The geometric area of the carbon paper was used to normalize the current density. The working electrode was prepared as followed. Base material carbon paper was first ultrasonic for 5 minutes in ethanol, 4M HNO₃ solution and deionized water, respectively. Air dry and ready for use. The **NiL₂-G** inks were prepared by sonicating 0.5mL acetonitrile, 0.5mL dimethylcarbinol and 3mg **NiL₂-G** for 2 hours. Then, using pipetting gun to accurately absorbed 50 μ L as-prepared inks and uniformly loaded onto the treated carbon paper with the area of 0.25cm² and dried under environmental condition. After that, protect and immobilize the catalyst by covering the surface with 2 μ L Nafion (5 % in 2-propanol) solution. The preparation of **NiL₂-R**

electrode is similar to **NiL₂-G**. In addition to keep the carbon paper in 140°C oven for 2 hours after loading the **NiL₂-R** ink onto the carbon paper. The method of preparing **CB@NiL₂** ink is almost the same as above but with additional appropriate amount of carbon black (CB) while preparing. The working electrodes underwent 20 cycles of cycle voltammetry until stabilization of current before data collection. Electrochemical impedance spectroscopy (EIS) measurements of the catalysts were conducted at a potential of 1.65 V vs RHE in a frequency range from 10⁵ Hz to 1 Hz by using an AC voltage with 5 mV amplitude. Double layer capacitance (C_{dl}) of all the as-obtained samples was measured in 1 M KOH solution. Then, five CVs with different scan rates (20, 40, 60, 80, 100 and 120 mV·s⁻¹) were obtained in a potential range of 0.1 to 0.2 V, in which no Faradaic process occurs and the current emerges mainly from the double layer capacitance.

Table S1 Strategy of transition metal complexes as electrocatalysts for OER.

Strategy	Structure	Title	Reference
Immobilization of metal complexes on micropore materials as heterogeneous catalyst	 <p>MTPP-CNT/CB</p>	Enhanced Catalytic Activity of Cobalt Porphyrin in CO ₂ Electroreduction Upon Immobilization on Carbon Materials	<i>Angew. Chem. Int. Ed.</i> , 2017 , 56, 6468-6472.
		Functionalized Carbon Nanotubes with Ni(II) Bipyridine Complexes as Efficient Catalysts for the Alkaline Oxygen Evolution Reaction	<i>ACS Catal.</i> , 2017 , 7, 8033-8041.
		A Mononuclear Co ^{II} Coordination Complex Locked in a Confined Space and Acting as an Electrochemical Water-Oxidation Catalyst: A “Ship-in-a-Bottle” Approach	<i>Angew. Chem. Int. Ed.</i> 2016 , 55, 2425 - 2430
directly fixed on the carbon paper as electrode		Heptanuclear Co, Ni and mixed Co-Ni clusters as high-performance water oxidation electrocatalysts	<i>Electrochimica Acta</i> , 2017, 249: 343-352.
Concomitant polymorphs of nickel complex as heterogeneous catalysts		Superior Performance Water Oxidation of Concomitant Polymorphic Crystals of a Mononuclear Nickel Complex	This work

Structure comparison and DFT Calculations

Table S2. DFT calculation on the coordinating OH⁻ mode of NiL₂-R and NiL₂-G.

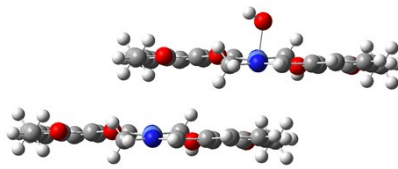
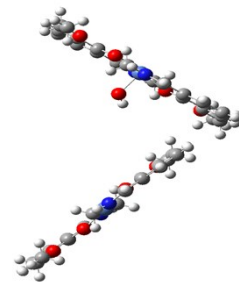
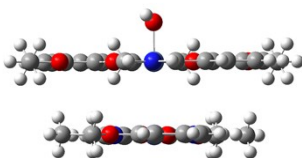
Model	Ni-Ni distance (Å)	structure
G1	6.239	
G2	9.445	
R2	3.357	

Table S3. Gibbs free energy of NiL₂ on different steps of OER under U=0 and 1.0 V.

U=0V						
GFE (eV)	NiL ₂	L ₂ Ni ^{III} -OH	L ₂ Ni ^{IV} =O	L ₂ Ni ^{III} -OOH	NiL ₂	
pH=14	G1	0.000	0.842	1.949	1.301	0.261
	G2	0.000	0.883	1.991	1.586	0.261
	R1	0.000	0.855	1.930	1.320	0.261
U=1V						
pH=14	G1	0.000	-0.158	-0.051	-1.699	-3.739
	G2	0.000	-0.117	-0.009	-1.414	-3.739
	R1	0.000	-0.145	-0.070	-1.680	-3.739

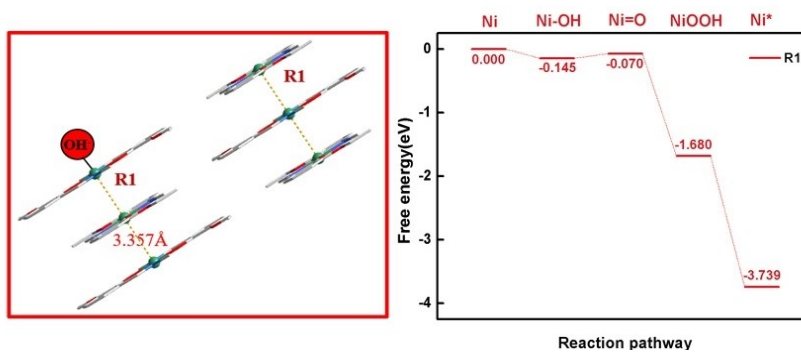


Figure S1. Gibbs free energy level diagram of different steps of OER on NiL₂-R.

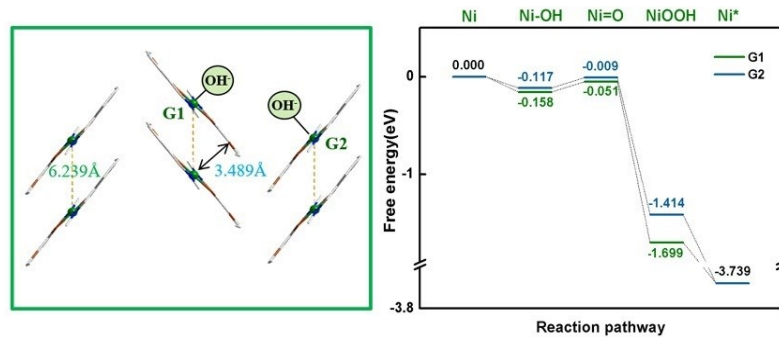


Figure S2. Gibbs free energy level diagram of different steps of OER on $\text{NiL}_2\text{-G}$.

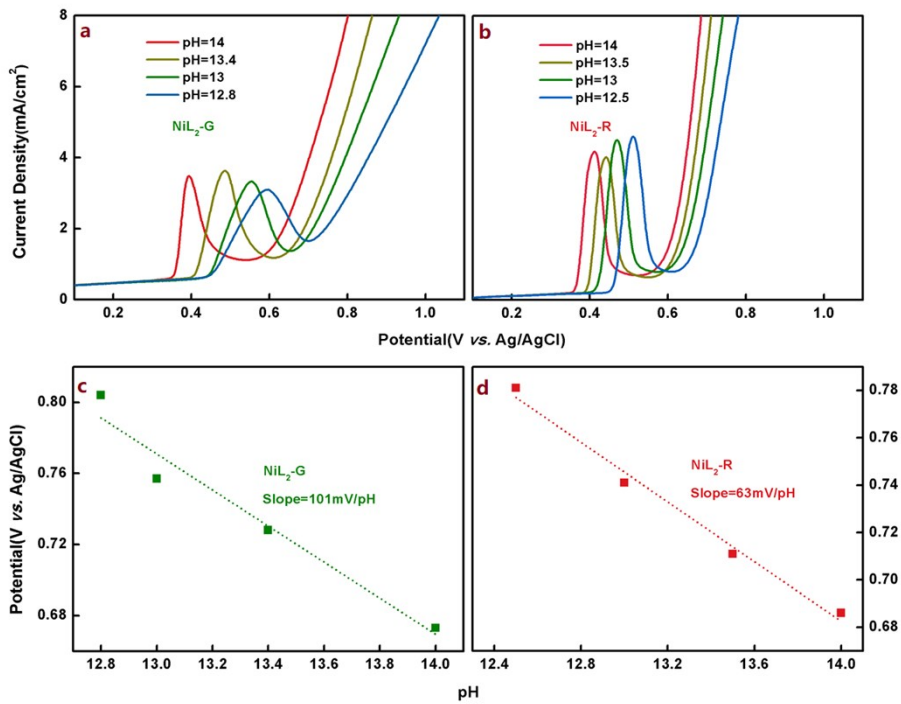


Figure S3. Half CVs of (a) $\text{NiL}_2\text{-G}$ and (b) $\text{NiL}_2\text{-R}$ electrodes in aqueous solutions with different pH values (the scan rate is 10mV/s). And the dependent potentials of (c) $\text{NiL}_2\text{-G}$ and (d) $\text{NiL}_2\text{-R}$ on pH values.

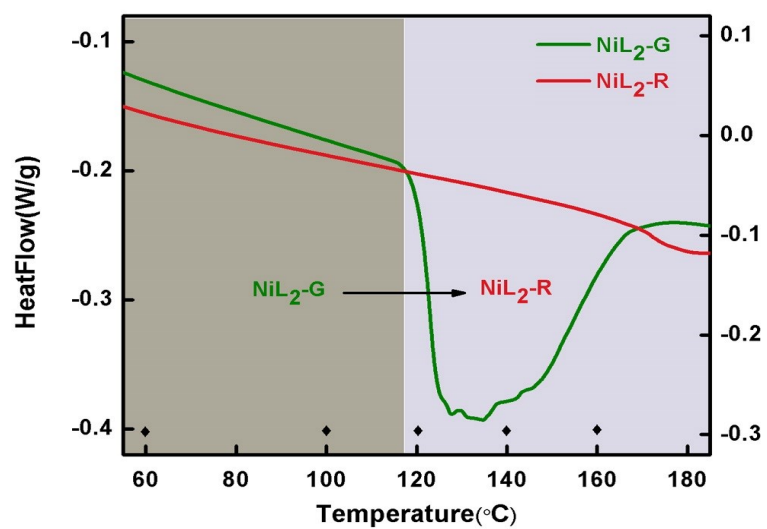


Figure S4. DSC curves (Normalized) of NiL₂-R than that of NiL₂-G.

Electrocatalytic oxygen evolution of NiL₂ electrode

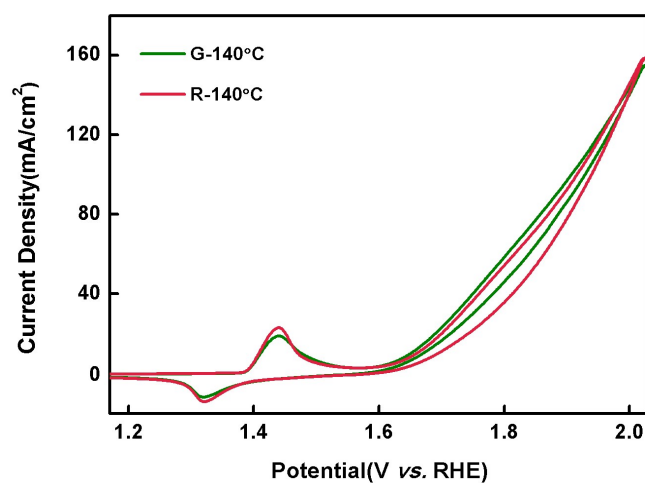


Figure S5 CVs for NiL₂-G and NiL₂-R treated at 140 °C for 2 hours

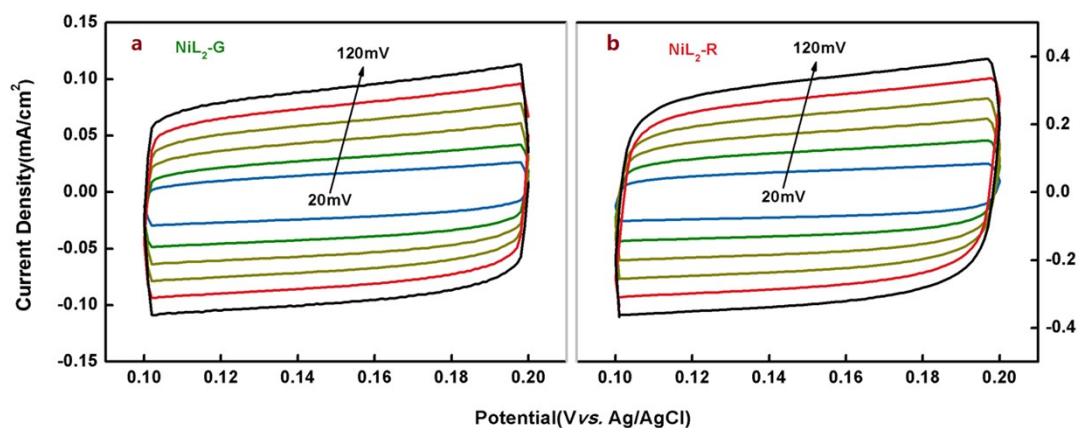


Figure S6 CVs were measured in the non-faradaic region of 0.10–0.20 V vs. Ag/AgCl with different scan rates, varying from 20 mV s⁻¹ to 120 mV s⁻¹.

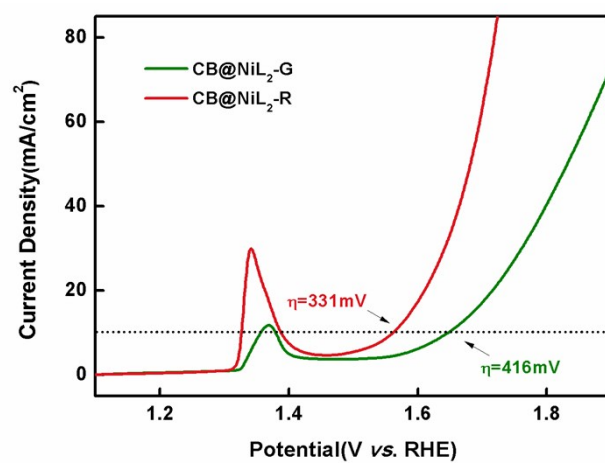


Figure S7 85% IR-corrected polarization LSV curves in 1.0 M KOH at a scan rate of 10 mV/s for CB@NiL₂-G and CB@NiL₂-R.

Table S4 Comparison of the parameters in our work with other reported examples.

Compound	Overpotential (mV) (10 mA/cm ²)	Tafel plots (mV/decade)	Reference
Co₇	410	72.9	[2]
Ni₇	400	55.5	
Ni_xCo_{7-x}	360	53.4	
Ni-POM	-	168.41	[3]
Co-WOC	-	128	[4]
Ni₆(PET)₁₂	430	69	[5]
Ni^{II}Se₄@GC	270	89	[6]
Ni-bipy-MWNT	290	35	[7]
NiL₂-G	466	185	Our work
NiL₂-R	339	98	Our work

Stability and Physical characterization of the NiL₂-G and NiL₂-R electrode



Figure S8 NiL₂-R soaked in KOH solution for 10 hours.

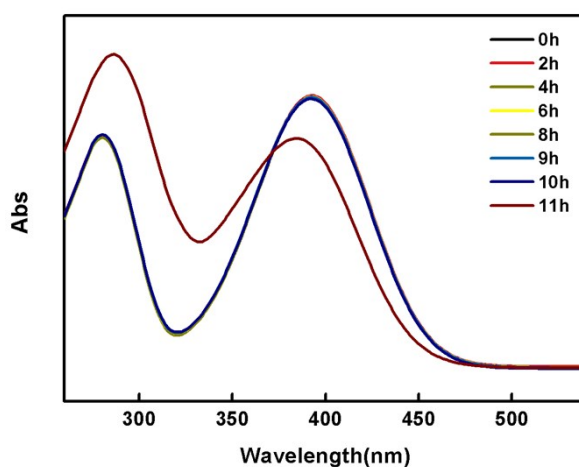


Figure S9 UV-vis absorption spectra along with the time for NiL₂ (1mg) dissolved in a mixture solvent of DMF (1mL) and KOH solution (9mL).

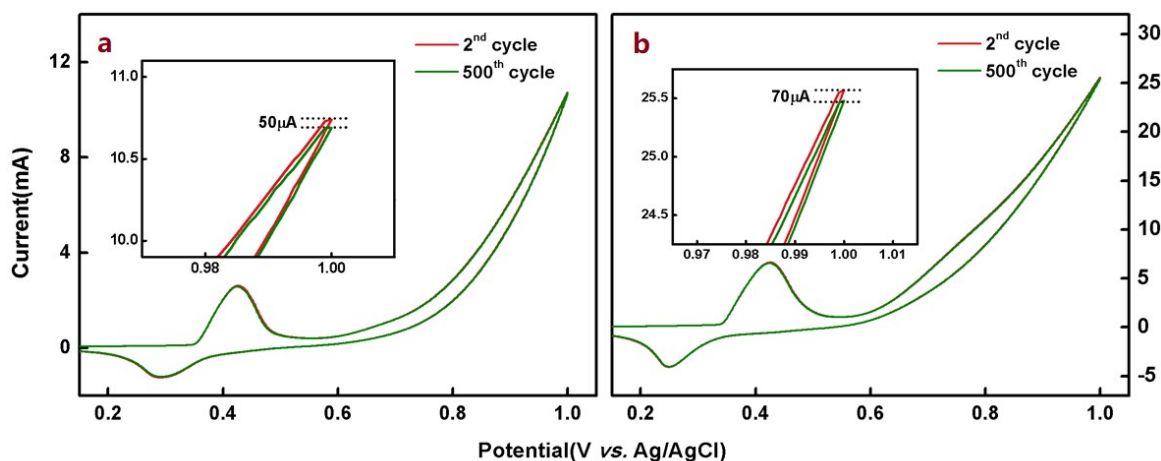


Figure S10 Stability check of NiL₂ by 500 cycles of CV scans in a 1 M KOH representing the (red) 2nd and (black) 500th cycles of the CV scan of NiL₂-G (a) and NiL₂-R (b). Inset: Enlarged region of the same voltammograms showing only a 50 μA difference for NiL₂-G and 70 μA difference for NiL₂-R in the catalytic current.

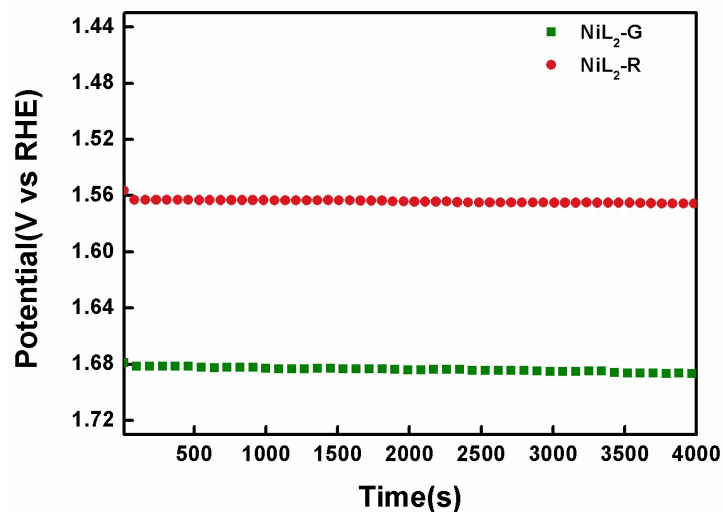


Figure S11 Chronopotentiometric measurements of NiL₂-G and NiL₂-R for 4000 seconds with a current density of 10mA/cm².

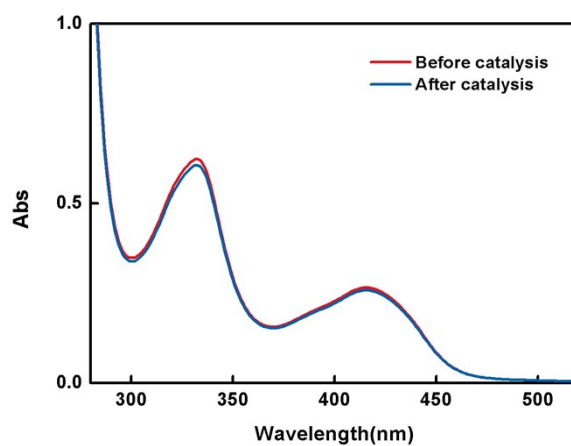


Figure S12 UV-vis absorption spectra of electrode materials dissolved in DMF before and after catalysis, show no obvious change in the curve.

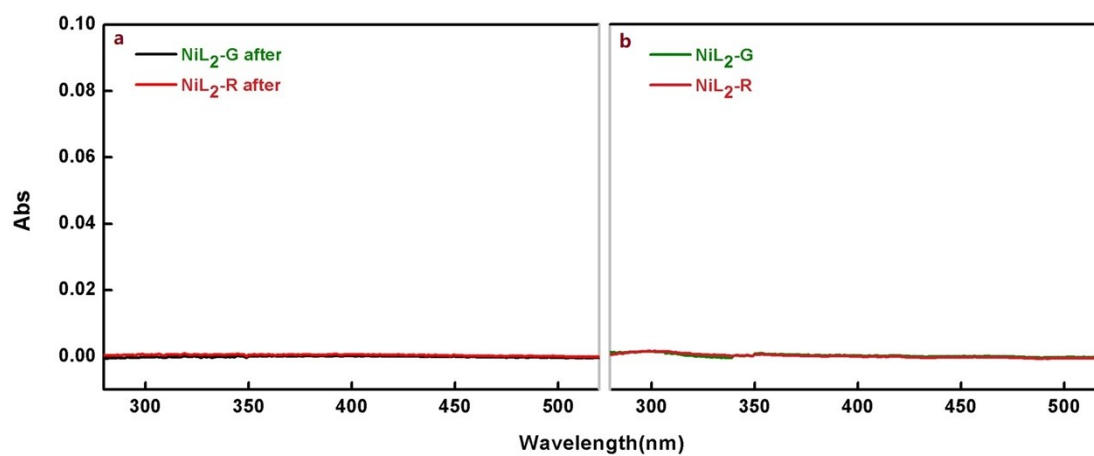


Figure S13 UV-vis absorption spectra of (a) the electrolyte and (b) the centrifuged products of electrolytes dissolved in DMF after catalysis.

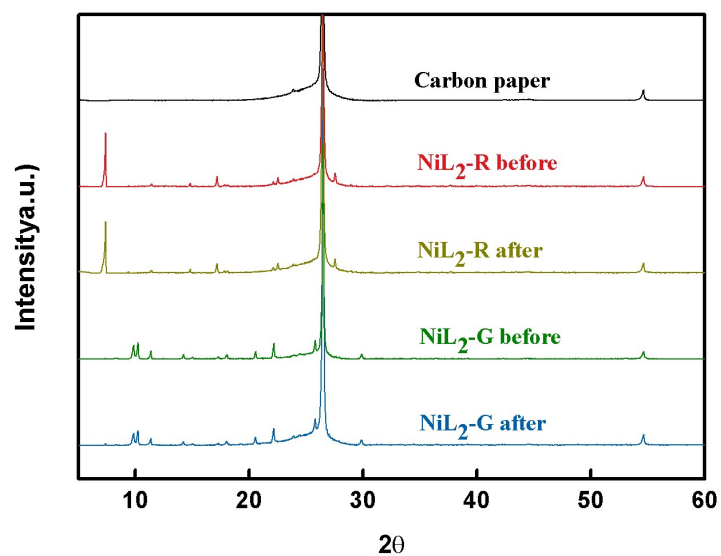


Figure S14 PXRD spectra for pure carbon paper, $\text{NiL}_2\text{-G}$ before and after catalysis, $\text{NiL}_2\text{-R}$ before and after catalysis.

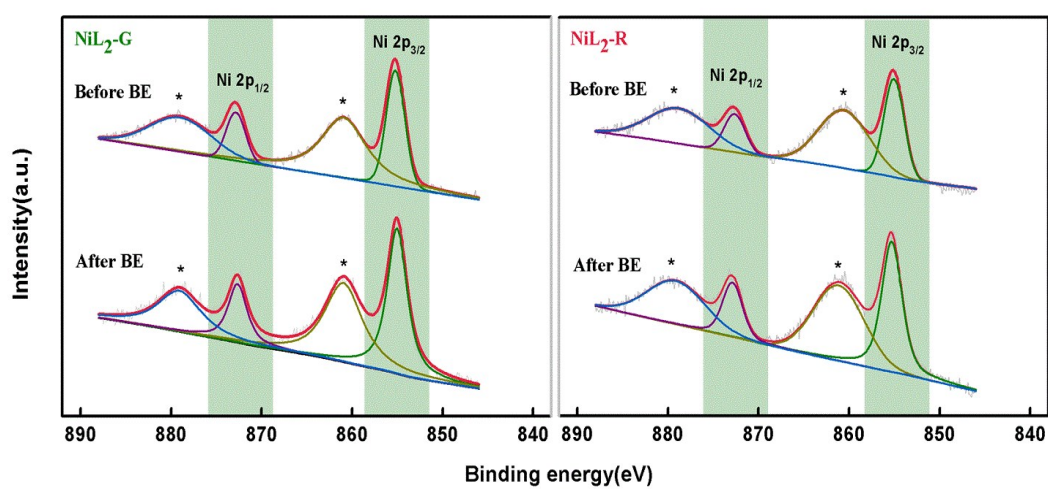


Figure S15 Comparison of the Ni 2p high-resolution XPS survey spectrum of $\text{NiL}_2\text{-G}$ (right) and $\text{NiL}_2\text{-R}$ (left) before and after electrocatalysis; The satellite peaks are indicated by an asterisk (*).

Reference

- [1] M. J. Frisch, G. W. Trucks, H. B. Schlegel, G. E. Scuseria, M. A. Robb, J. R. Cheeseman, G. Scalmani, V. Barone, G. A. Petersson, H. Nakatsuji, X. Li, M. Caricato, A. V. Marenich, J. Bloino, B. G. Janesko, R. Gomperts, B. Mennucci, H. P. Hratchian, J. V. Ortiz, A. F. Izmaylov, J. L. Sonnenberg, D. Williams-Young, F. Ding, F. Lipparini, F. Egidi, J. Goings, B. Peng, A. Petrone, T. Henderson, D. Ranasinghe, V. G. Zakrzewski, J. Gao, N. Rega, G. Zheng, W. Liang, M. Hada, M. Ehara, K. Toyota, R. Fukuda, J. Hasegawa, M. Ishida, T. Nakajima, Y. Honda, O. Kitao, H. Nakai, T. Vreven, K. Throssell, J. A. Montgomery, Jr., J. E. Peralta, F. Ogliaro, M. J. Bearpark, J. J. Heyd, E. N. Brothers, K. N. Kudin, V. N. Staroverov, T. A. Keith, R. Kobayashi, J. Normand, K. Raghavachari, A. P. Rendell, J. C. Burant, S. S. Iyengar, J. Tomasi, M. Cossi, J. M. Millam, M. Klene, C. Adamo, R. Cammi, J. W. Ochterski, R. L. Martin, K. Morokuma, O. Farkas, J. B. Foresman, and D. J. Fox, Gaussian, Inc., Wallingford CT, 2016.
- [2] D. Cai, A. Han, P.-Y. Yang, Y.-F. Wu, P. Du, M. Kurmoo, M.-H. Zeng, Heptanuclear Co, Ni and mixed Co-Ni clusters as high-performance water oxidation electrocatalysts, *Electrochim. Acta*, 2017, **249**, 343-352.
- [3] C. Singh, S. Mukhopadhyay, and S. K. Das, Polyoxometalate-Supported Bis(2,2'-bipyridine)mono(aqua)nickel(II) Coordination Complex: an Efficient Electrocatalyst for Water Oxidation, *Inorg Chem.*, 2018, **57**, 6479-6490.
- [4] P. Manna, J. Debgupta, S. Bose, and S. K. Das, A Mononuclear Co^{II} Coordination Complex Locked in a Confined Space and Acting as an Electrochemical Water-Oxidation Catalyst: A "Ship-in-a-Bottle" Approach, *Angew. Chem. Int. Ed.*, 2016, **128**, 2471-2476.
- [5] D. R. Kauffman, D. Alfonso, D. N. Tafen, J. Lekse, C. Wang, X. Deng, J. Lee, H. Jang, J. Lee, S. Kumar, C. Matranga, Electrocatalytic Oxygen Evolution with an Atomically Precise Nickel Catalyst, *ACS Catal.*, 2016, **6**, 1225-1234.
- [6] J. Masud, P.-C. Ioannou, N. Levesanos, P. Kyritsis, and M. Nath, A Molecular Ni-complex Containing Tetrahedral Nickel Selenide Core as Highly Efficient Electrocatalyst for Water Oxidation, *ChemSusChem*, 2016, **9**, 3128-3132.
- [7] M. Tavakkoli, M. Nosek, J. Sainio, F. Davodi, T. Kallio, P. M. Joensuu, K. Laasonen, Functionalized Carbon Nanotubes with Ni(II) Bipyridine Complexes as Efficient Catalysts for the Alkaline Oxygen Evolution Reaction, *ACS Catal.*, 2017, **7**, 8033-8041.